JACS
JOURNAL OF THE AMERICAN CHEMICAL SOCIETY

ARTICLE

pubs.acs.org/JACS

Silylation of Iron-Bound Carbon Monoxide Affords a Terminal Fe Carbyne

Yunho Lee and Jonas C. Peters*

Division of Chemistry and Chemical Engineering, California Institute of Technology, Pasadena, California 91125, United States

Supporting Information

ABSTRACT: A series of monocarbonyl iron complexes in the formal oxidation states 0, +1, and +2 are accessible when supported by a tetradentate tris(phosphino)silyl ligand (SiP^{iPr}_3 = $[Si(o\text{-}C_6H_4PiPr_2)_3]^-$). X-ray diffraction (XRD) studies of these carbonyl complexes establish little geometrical change about the iron center as a function of oxidation state. It is possible to functionalize the terminal CO ligand of the most reduced carbonyl adduct by addition of $SiMe_3^+$ to afford a well-defined iron carbyne species, $(SiP^{iPr}_3)Fe{\equiv}C{-}OSiMe_3$. Single-crystal XRD data of this iron carbyne derivative reveal an unusually short $Fe{\equiv}C{-}OSiMe_3$ bond distance (1.671(2) Å) and a substantially elongated C−O distance (1.278(3) Å), consistent with Fe−C carbyne character. The overall trigonal bipyramidal geometry of $(SiP^{iPr}_3)Fe{\equiv}C{-}OSiMe_3$ compares well with that of the corresponding carbonyls, $(SiP^{iPr}_3)Fe(CO)^-$, $(SiP^{iPr}_3)Fe(CO)$, and $(SiP^{iPr}_3)Fe(CO)^+$. Details regarding the electronic structure of the carbyne complex have been explored via the collection of comparative Mössbauer data for all of the complexes featured and also via DFT calculations. In sum, these data point to a strongly π-accepting Fischer-type carbyne ligand that confers stability to a low-valent iron(0) rather than high-valent iron(IV) center.

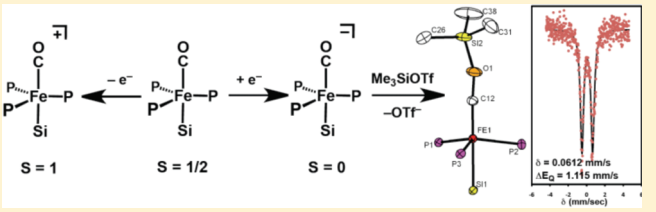

INTRODUCTION

There has been a surge of interest in the chemistry of low-valent, redox-active complexes of the mid-to-late first-row transition metals in recent years.[1,2] This interest has been in part motivated by a desire to generate species that feature uncommon metal-to-ligand multiply bonded species such as oxos, imides, and nitrides via partial or complete group transfer. The study of such species will help to expose the respective roles they might play in small-molecule transformations that include, for example, nitrogen reduction, C−H oxygenations and aminations, and aziridinations.[3,4] With these goals in mind, our group recently introduced "$(SiP^R_3)Fe$" (where SiP^R_3 = $[Si(o\text{-}C_6H_4PPh_2)_3]^-$ or $[Si(o\text{-}C_6H_4PiPr_2)_3]^-$ for R = Ph and ^{i}Pr, respectively) as a versatile low-valent iron scaffold that can accommodate a range of ligands in an axial fifth site trans to the silyl anchor. A salient example concerns the ligand N_2, where terminally bonded $(SiP^{iPr}_3)Fe{-}N_2$ complexes can be accessed in three formal iron oxidation states (0, +1, +2), and reductive functionalization of the terminally bonded N_2 ligand is possible.[4,5] It was of interest to us to explore whether a parallel manifold of chemistry might also be accessible for carbon monoxide. A conceptual link between the chemical reduction of CO and N_2 is well appreciated within the organometallic community.[6] The very recent discovery that VFe-nitrogenase enzymes can catalyze CO reduction to higher order carbon chains when the N_2 substrate is replaced by CO lends new motivation to comparative studies along this line of inquiry.[7]

In this paper we establish the utility of the $(SiP^{iPr}_3)Fe$ scaffold in supporting a series of isostructural CO complexes that span the formal oxidation states $Fe^0{-}CO$, $Fe^I{-}CO$, and $Fe^{II}{-}CO$. Silylation of the terminal $Fe^0{-}CO$ species affords access to a well-defined and structurally unusual Fischer-type carbyne complex,[8,9] $(SiP^{iPr}_3)Fe(COSiR_3)$, with a distinctly short Fe−C bond distance (ca. 1.67 Å). Fischer and co-workers have reported the singular previous example of a structurally characterized carbyne complex of iron.[10] Because the mode by which the featured carbyne is generated can, in principle, be regarded as a net four-electron reduction with concomitant partial O-atom transfer, it is of interest to consider the relative states of oxidation of the structurally similar iron CO and carbyne complexes described herein. Comparative Mössbauer and DFT data are presented to shed light on this issue.

RESULTS AND DISCUSSION

Monovalent, yellow $(SiP^{iPr}_3)Fe(CO)$ (**1**) is accessible by ligand substitution (>90% yield) from the previously reported N_2 adduct species $(SiP^{iPr}_3)Fe(N_2)$[4] by CO(g) (eq 1). An X-band EPR spectrum of **1** at 77 K in 2-MeTHF/THF (1:9) reveals a nearly axial signal (see Supporting Information), in accord with solution magnetic data (μ_{eff} = 2.2 μ_B in C_6D_6 at 22 °C) for an S = 1/2 species. Complexes in which a terminal carbonyl and a silyl

Received: October 27, 2010
Published: March 04, 2011

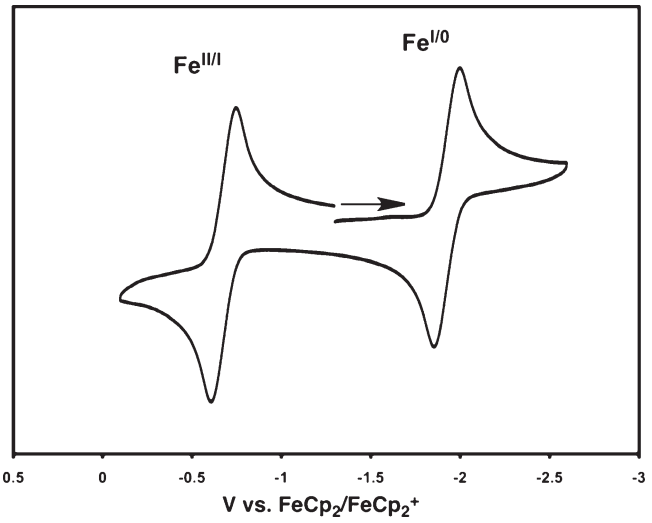

Figure 1. Cyclic voltammogram of $(SiP^{iPr}_3)Fe(CO)$ (**1**); scan rate = 100 mV/s. $Fe^{II/I}$ couple at −0.68 V and $Fe^{I/0}$ couple at −1.93 V vs Fc/Fc^+ were observed in THF with 0.3 M tetra-*n*-butylammonium hexafluorophosphate as an electrolyte.

ligand are *trans* disposed, as they are in **1** ($\angle$SiFeC = 178.7(2)°), are uncommon.[11,12] The cyclic voltammetry of **1** (Figure 1) is interesting in that it reveals two reversible one-electron redox couples, consistent with the electrochemical generation of the $Fe{-}CO^+$ cation at −0.68 V and its corresponding anion $Fe{-}CO^-$ at −1.9 V (versus Fc/Fc^+). We were thus encouraged to pursue the chemical generation of both the anion and the cation of **1**.

$$(SiP^{iPr}_3)Fe{-}N_2 + CO \rightarrow (SiP^{iPr}_3)Fe - CO + N_2 \qquad (1)$$

Chemical reduction of a yellow solution of **1** effects a dramatic color change to an inky red, and subsequent workup affords the diamagnetic ion-paired species $(SiP^{iPr}_3)Fe(CONa(THF)_3)$ (**2**) in approximately quantitative yield (Scheme 1). As is to be expected, the ν(CO) at 1717 cm^{-1} (KBr pellet; ^{13}CO = 1676 cm^{-1}) is substantially lower than that of neutral **1** (1850 cm^{-1}; ^{13}CO = 1806 cm^{-1}) owing to an increase in π-back-donation. Addition of two equiv of 12-crown-4 to **2** fully encapsulates the Na^+ cation to afford the terminally bonded, anionic CO adduct, $\{Na(12\text{-}C\text{-}4)_2\}\{(SiP^{iPr}_3)Fe(CO)\}$ (**3**) (KBr pellet; ν(CO) = 1757 cm^{-1}; ^{13}CO = 1713 cm^{-1}). The X-ray structures of **1** and **2** are shown in Figure 2. Neutral **1** is isostructural to its corresponding N_2 derivative (see Figure 2a and Table 1).[4] Ion-paired **2** reveals a crystallographically imposed three-fold axis and hence an essentially perfect trigonal bipyramidal (TBP) structure type (τ = 1.0).[13] The Fe−C bond distance contracts appreciably to 1.732(3) Å in **2** compared with that for neutral **1** (1.769(2) Å, Table 1), and there is modest elongation of the CO bond (1.188(3) Å in **2** vs 1.169(2) Å in **1**).

Derivatization of the CO ligand via addition of trimethylsilyl trifluoromethanesulfonate to a frozen THF solution of **2** affords the featured carbyne complex $(SiP^{iPr}_3)Fe(COSiMe_3)$ (**4**) as a red solid. The ^1H NMR spectrum of diamagnetic **4** features a new resonance at 0.34 ppm for the $-SiMe_3$ group. The ^{31}P NMR spectrum of **4** shows a singlet at 104.6 ppm, which splits into a doublet in a ^{13}C-enriched sample ($^2J_{CP}$ = 16.3 Hz, Figure 3a) owing to coupling to the $-COSiMe_3$ C-atom. A quartet at

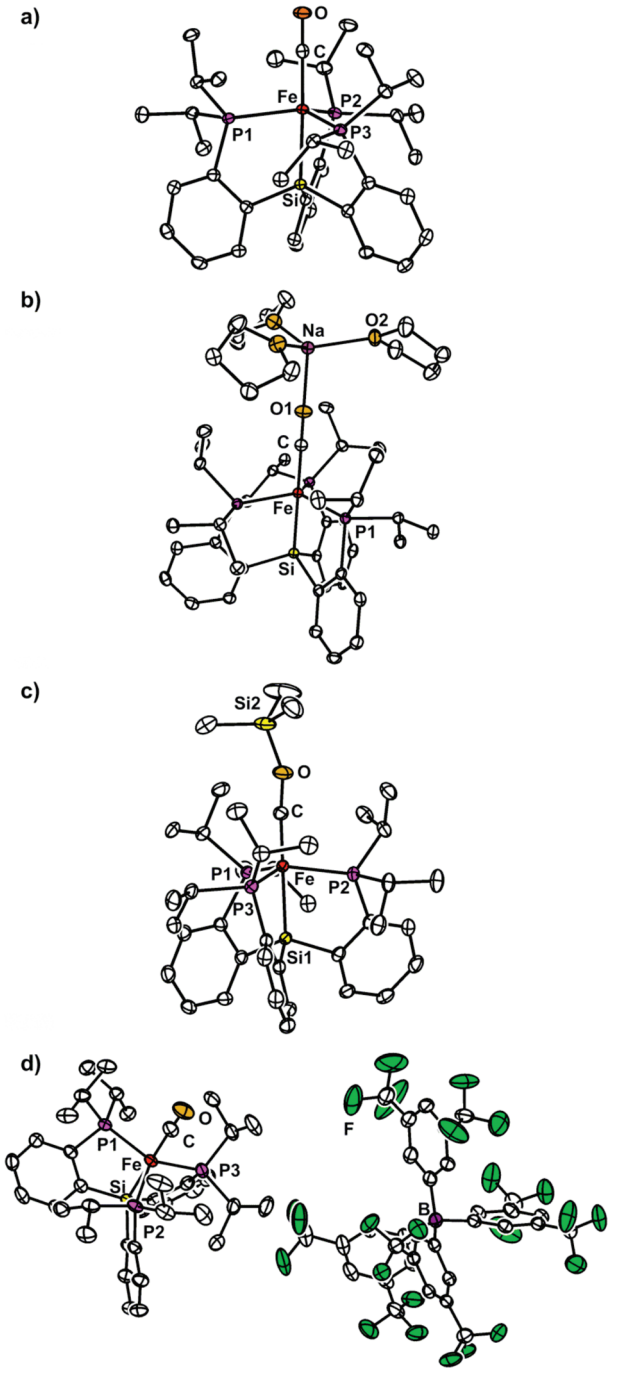

Figure 2. Displacement ellipsoid (50%) representations of (a) $(SiP^{iPr}_3)Fe(CO)$ (**1**), (b) $(SiP^{iPr}_3)Fe(CONa(THF)_3)$ (**2**), (c) $(SiP^{iPr}_3)Fe(COSiMe_3)$ (**4**), and (d) $\{(SiP^{iPr}_3)Fe(CO)\}\{B(Ar^F)_4\}$ (**5**). Hydrogen atoms and molecules of co-crystallization are omitted for clarity.

250.3 ppm (q, $^2J_{CP}$ = 16.4 Hz, Figure 3b) in the ^{13}C NMR spectrum demonstrates ^{13}C coupling to three equivalent phosphorus atoms to cement this assignment. This resonance shifts downfield by ~10 ppm from that of its corresponding precursor complex **2**. Two ^{29}Si NMR signals were detected for **4** at 94.5 (q, $^2J_{SiP}$ = 40 Hz) and 20.3 (s) ppm, corresponding to the Si atoms in the SiP^{iPr}_3 and TMS units, respectively. These peaks reveal $^{29}Si{-}^{13}C$ coupling in a ^{13}C-enriched sample: 94.3 (dq, $^2J_{SiP}$ =

dx.doi.org/10.1021/ja109678y |J. Am. Chem. Soc. 2011, 133, 4438–4446

Table 1. Physical Parameters for the Species 1, 2, 4, and 5

	{FeCO}{B(Ar^F)$_4$}^{d} (**5**)	Fe−CO (**1**)	Fe{CONa(THF)$_3$} (**2**)	Fe(COSiMe$_3$)^e (**4**)
ν(CO) (cm^{-1})^a	1943	1852	1711	−
ν(CO) (cm^{-1})^b	1959	1850	1717	−
C−O (Å)	1.102(4)	1.169(2)	1.188(3)	1.278(3)
Fe−C (Å)	1.842(3)	1.769(2)	1.732(3)	1.671(2)
Fe−Si (Å)	2.3245(7)	2.2942(4)	2.2586(8)	2.2973(6)
C−O−X (°)	−	−	180.000(1)	155.0(2)
Si−Fe−C (°)	178.69(9)	178.04(5)	180.000(1)	177.90(7)
τ	0.99	0.95	1	0.98
spin-state^c	2.7 μ_B, S = 1	2.0 μ_B, S = 1/2	diamagnetic	diamagnetic

^{a} In THF. ^{b} In KBr pellet. ^{c} Evans method in THF-d_8. ^{d} B(Ar^F)$_4$ = B(3,5-(CF$_3$)$_2$-C$_6$H$_3$)$_4$. ^{e} Contains **1**.

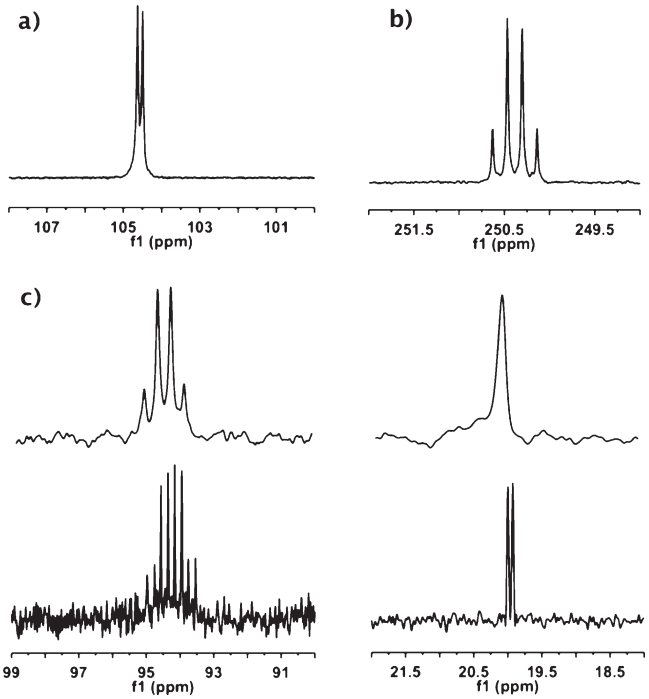

Figure 3. Multinuclear NMR data of (SiP$^{i\mathrm{Pr}}{}_3$)Fe(COSiMe$_3$) (**4**): (a) ^{31}P NMR spectrum of (SiP$^{i\mathrm{Pr}}{}_3$)Fe(^{13}COSiMe$_3$) (**4-^{13}CO**), (b) ^{13}C NMR spectrum of (SiP$^{i\mathrm{Pr}}{}_3$)Fe(^{13}COSiMe$_3$) (**4-^{13}CO**), and (c) ^{29}Si NMR spectra of (SiP$^{i\mathrm{Pr}}{}_3$)Fe(COSiMe$_3$) (**4**, top) and (SiP$^{i\mathrm{Pr}}{}_3$)Fe(^{13}COSiMe$_3$) (**4-^{13}CO**, bottom). All spectra were measured in C$_6$D$_6$ at room temperature.

40 Hz, $^2J_{SiC}$ = 21 Hz) and 20.0 (d, $^2J_{SiC}$ = 7 Hz) ppm. Representative NMR data are collected in Figure 3.

The solid-state structure of **4** (Figure 2c) establishes the five-coordinate TBP (τ = 0.91) geometry at the iron center with an η^1-bound "COSiMe$_3$" ligand. The Fe−C bond distance is unusually short (1.671(2) Å), and the C−O distance is substantially elongated (1.278(3) Å) in comparison to **1** and **2**, consistent with Fe−C carbyne character. Indeed, the Fe−C distance in **4** is appreciably shorter than that of Fischer's original iron aminomethylidyne complex (1.734(6) Å).[10a] The Si−O distance is 1.674(2) Å, consistent with Si−O distances of structurally related RMe$_2$Si−O−C≡N and other terminal siloxycarbyne metal complexes,[14,15] and the ∠C−O−Si angle is 155.0(2)°. The 1.278(3) Å C−O bond distance can be compared to C−O single bonds in the few structurally characterized

Scheme 1

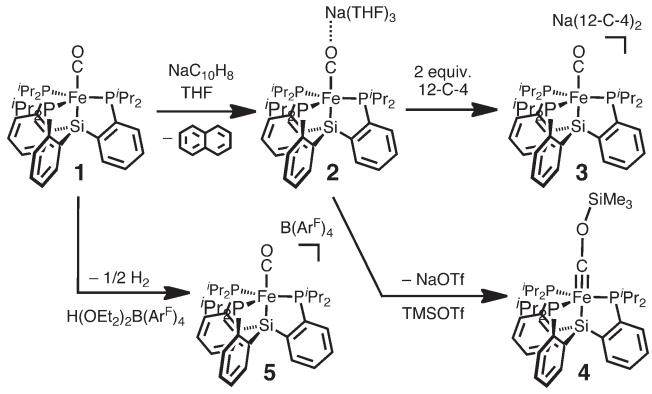

organic alkynyl ether molecules with a C≡C−O−X-type linkage.[16] Stang has, for example, structurally determined that the acetylenic−oxygen C(sp)−O bond distance in −C≡C−O−SO$_2$R-type derivatives is far shorter (ca. 1.33 Å) than in corresponding but saturated alkyl C(sp^3)−O species, where the distance is ca. 1.46 Å.[16a] DFT data for **4** also support the multiple bond character of the Fe−C bond (vide infra).[17]

Because the generation of the featured carbyne can, in principle, be regarded as a net four-electron CO reduction with concomitant partial O-atom transfer to Si, it is of interest to consider the relative states of oxidation of the structurally related Fe−CO and carbyne complexes under present consideration. The electronic structure of carbyne **4** is perhaps most interesting in this context. If one assigns an oxidation state to its iron center by removal of all ligands in their closed-shell configurations (i.e, {SiP$^{i\mathrm{Pr}}{}_3$}$^-$ and {COSiMe$_3$}$^{3-}$),[18] an Fe(4+) d^4 assignment is suggested. This scenario draws analogy between **4** and several three-fold symmetric L$_3$Fe≡N$_x$ species that have been characterized, where N$_x$ = NR^{2-} or N^{3-}.[3c,19] However, one can alternatively regard the carbyne ligand as a {COSiMe$_3$}$^+$ closed-shell cation, akin to the {CONa}$^+$ ligand of **2**, with one σ-donor and two π-acceptor orbitals at carbon. This formulation is more suggestive of "Fischer-type" carbyne character, where the polarization is inverted and the iron center back-donates to carbon. In this limit, the iron center is better described as low-valent d^8 iron(0). A final scenario worthy of mention is one where the tris(phosphino)silyl ligand is also regarded as a cation, {SiP$^{i\mathrm{Pr}}{}_3$}$^+$. Appreciating the high degree of covalent bonding in **4**, and hence the limited utility of assigning the number of "d" electrons present, we conducted comparative

dx.doi.org/10.1021/ja109678y |J. Am. Chem. Soc. 2011, 133, 4438–4446

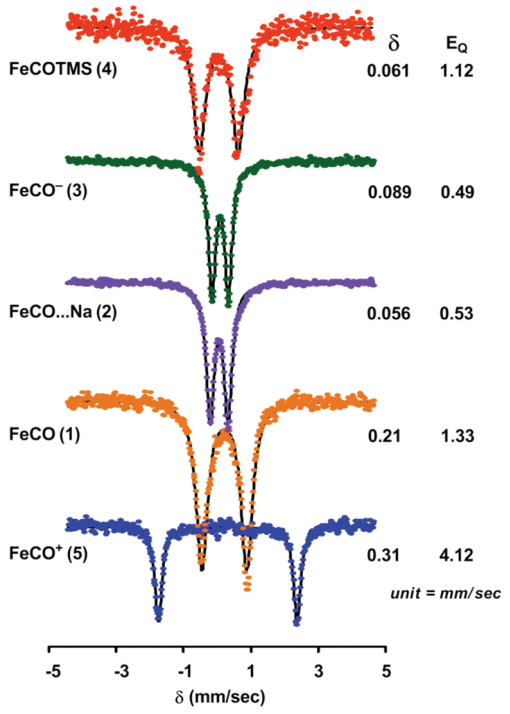

Figure 4. Zero-field Mössbauer spectra of $(SiP^{iPr}_3)Fe(CO)$ (**1**), $(SiP^{iPr}_3)Fe(CONa(THF)_3)$ (**2**), $\{Na(12\text{-}C\text{-}4)_2\}\{(SiP^{iPr}_3)Fe(CO)\}$ (**3**), $(SiP^{iPr}_3)Fe(COSiMe_3)$ (**4**), and $\{(SiP^{iPr}_3)Fe(CO)\}\{B(Ar^F)_4\}$ (**5**) recorded at 77 K.

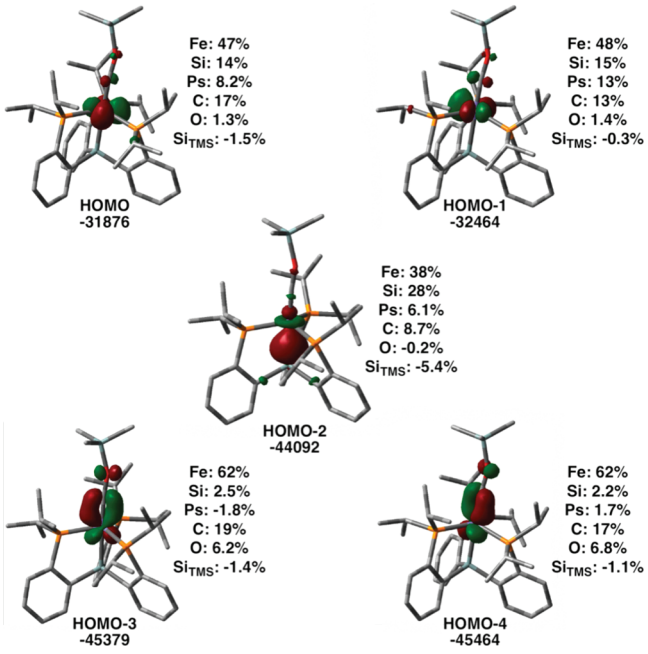

Figure 5. HOMO − HOMO-4 of $(SiP^{iPr}_3)Fe(COSiMe_3)$ (**4**) derived from the single-point DFT calculations with corresponding Mulliken populations (see Experimental Section); energies in cm^{-1}. Lobal representations correspond to the orbitals indicated by the number with 0.07 isocontours.

Mössbauer measurements on **1**−**4**. We also prepared the cationic, blue, and $S = 1$ Fe(II) carbonyl, $\{(SiP^{iPr}_3)Fe(CO)\}\{B(Ar^F)_4\}$ (**5**) (μ_{eff} = 2.69 μ_B, benzene, ν(CO) = 1959 cm^{-1} (^{13}CO = 1915 cm^{-1}), KBr pellet), by oxidation of **1** with $H(OEt_2)_2$-$[B(3,5\text{-}(CF_3)_2\text{-}C_6H_3)_4]$ for additional comparison (Scheme 1). Complex **5** is an unusual example of a terminal carbonyl adduct that populates a triplet ground state.[20]

Figure 4 overlays the Mössbauer spectra for **1**−**5**. Although the isomer shift can often be identified with a particular Fe valence state, strong covalency can compress the range of isomer shifts and thereby not give a definitive indication of the iron valence. In addition, the local geometry of an iron center impacts both isomer shift and quadropole splitting parameters.[21−23] It is therefore most instructive to internally compare the present set of data, where the geometry at iron is highly conserved and only the axial ligand and overall molecular charge is altered. As can be gleaned from Figure 4, the isomer shifts of the various compounds are positive and compressed over a rather narrow range. This fact intimates that much of the redox/charge-transfer chemistry occurs at the terminal $CO/COSiMe_3$ ligands in this series of complexes, presumably via relative π-back-bonding contributions from iron that are compensated by its σ-accepting contribution. Comparison of the isomer shifts of the terminally bonded carbonyl adducts $Fe{-}CO^-$ **3**, Fe−CO **1**, and $Fe{-}CO^+$ **5** expectedly shows that the isomer shift δ for these three complexes shifts positive (δ +0.09 (**3**), +0.21 (**1**), +0.31 (**5**)) as the overall molecular charge, and hence the relative state of iron oxidation, shifts positive from formal Fe(0) to Fe(I) to Fe(II). The trend reflects a decrease in s-electron density at Fe as electrons are successively removed from the system. The carbyne complex **4** affords an isomer shift (δ +0.06) that is almost indistinguishable from that of **2**, supporting the $\{C{-}O{-}Na\}^+$/$\{C{-}O{-}SiMe_3\}^+$ analogy drawn above. This fact appears to rule out the plausibility of the Fe(IV) d^4 configuration. It is interesting, therefore, to compare the isomer shifts of **2**, **3**, and **4** to those that have been reported for other five-coordinate, d^8 TBP complexes featuring a high degree of covalency due to combinations of CO and phosphine ligands. Such data have been tabulated in several studies for d^8 $[Fe(CO)_4(L)]$ species, where L for example is CO, PR_3, and $P(OR)_3$.[21,24−26] The isomer shifts of such d^8 TBP $[Fe(CO)_4(L)]$ structure types generally fall within a range of δ −0.09 (e.g., $Fe(CO)_5$) to −0.18 (e.g., $[Fe(CO)_4(SiCl_3)][Bu_4N]$[27]). While the isomer shift values for **2**, **3**, and **4** are somewhat more positive, they are in a reasonable range for the d^8 configuration given slight geometric variability, in addition to the presence of a $(SiP^{iPr}_3)Fe$ fragment that is chemically distinct from "$Fe(CO)_4$". Moreover, comparison of neutral **1** with neutral **4** shows a substantial decrease in the isomer shift value as the $SiMe_3$ group is added to the CO O-atom, again consistent with formal reduction of the iron center from d^7 to d^8. As a final point of comparison, we have recently reported Mössbauer data for an isostructural and isoelectronic series of $Fe{-}N_2$ and $Fe{-}N_2SiMe_3$ species supported by the (SiP^{iPr}_3) ligand.[5] The complex $(SiP^{iPr}_3)Fe(N_2SiMe_3)$ is isoelectronic with carbyne **4** and was likewise formulated as d^8. Its isomer shift is appreciably positive (δ +0.19) relative to **4**, presumably reflecting the higher electronegativity of nitrogen relative to carbon, and hence greater covalency in the Fe−C interaction relative to the Fe−N interaction. While the isomer shifts of the series $Fe{-}N_2^-$, $Fe{-}N_2$, $Fe{-}N_2^+$, and $Fe(N_2SiMe_3)$ follow the same trend observed for $Fe{-}CO^-$, Fe−CO, $Fe{-}CO^+$, and $Fe(COSiMe_3)$, they are all shifted positive and fall within the range from +0.18 ($Fe(N_2SiMe_3)$) to +0.53 ($Fe{-}N_2^+$). The very similar

dx.doi.org/10.1021/ja109678y |J. Am. Chem. Soc. 2011, 133, 4438–4446

Table 2. Selected Bond Indices and Bond Orbital Occupancies from Natural Bond Orbital Analysis

	$\{FeN_2\}\{NaTHF_3\}$	FeN_2TMS	$\{FeCO\}\{NaTHF_3\}$	FeCOTMS
		Wiberg Bond Index		
Fe−L	1.1051	1.4849	1.4845	1.8569
L−L′	2.3702	1.8371	1.6177	0.6766[a]
L′−Na or Si	0.0856	0.7609	0.0384	0.5236
Fe−Si	0.7294	0.6768	0.7115	0.7808
		Bond Orbital Occupancy		
Fe−L	1.93622 (20.43% Fe, 79.57% N)	1.94325 (21.03% Fe, 78.97% N)	1.85804 (34.37% Fe, 65.63% C)	1.88259 (35.86% Fe, 64.14% C)
		1.79698 (53.11% Fe, 46.89% N)		1.73379 (67.84% Fe, 32.16% C)
		1.79025 (49.38% Fe, 50.62% N)		1.73122 (69.19% Fe, 30.81% C)
L−L′	1.99372 (53.73% N, 46.27% N)	1.98931 (47.80% N, 52.20% N)	1.99089 (27.53% C, 72.47% O)	1.98781 (22.88% C, 77.12% O)
	1.99372 (53.73% N, 46.27% N)			
	1.99065 (48.96% N, 51.04% N)			
Fe−Si	1.61953 (54.43% Fe, 45.57% Si)	1.63573 (56.44% Fe, 43.56% Si)	1.61800 (55.48% Fe, 44.52% Si)	1.64338 (59.08% Fe, 40.92% Si)
Fe−P	1.81913 (27.88% Fe, 72.12% P)	1.84746 (31.78% Fe, 68.22% P)	1.80671 (30.59% Fe, 69.41% P)	1.84533 (35.09% Fe, 64.91% P)
	1.81921 (27.89% Fe, 72.11% P)	1.84705 (31.52% Fe, 68.48% P)	1.80666 (30.59% Fe, 69.41% P)	1.84533 (35.15% Fe, 64.85% P)
	1.81920 (27.89% Fe, 72.11% P)	1.85138 (31.21% Fe, 68.79% P)	1.80667 (30.59% Fe, 69.41% P)	1.84533 (35.35% Fe, 64.65% P)
Fe (LP)	1.83706	1.88808	1.84666	1.88179
	1.83698	1.88710	1.84652	1.88382
	1.64537		1.67127	
	1.64532		1.67118	

[a] Wiberg bond indices of free CO and N_2 reveal 2.1834 and 3.0493, respectively. The bond indices for C≡C and C−O bonds in propynyl tosylate[11a] are 2.6761 and 1.0649, respectively. Geometry optimization and NBO analysis for propynyl tosylate were run on the Gaussian03 suite of programs with the B3LYP level of theory with the 6-311G** basis set for all atoms.

quadrupole splitting values for carbyne **4** (E_Q = 1.11 mm/s) and $(SiP^{iPr}_3)Fe(N_2SiMe_3)$ (E_Q = 1.26 mm/s) further establish their close electronic structure relationship.

On the basis of these experimental data, we favor a simplistic limiting assignment of iron(0) d^8 for **4**, but DFT analysis of this complex forces us to further consider the iron(2−) d^{10} scenario. As illustrated by Figure 5, the five highest filled orbitals of **4** all have significant iron d-orbital character. For example, the HOMO is ca. 47% Fe and 17% $C_{carbyne}$ in character.[28] The HOMO-2 orbital in **4**, of approximate a_1 symmetry, is strongly mixed between Fe $3d_{z^2}/4s$ and (SiP^{iPr}_3) Si $5p_z$ (ca. 38% Fe and 28% Si) and hence cannot be reliably assigned to either iron or the (SiP^{iPr}_3) ligand. We therefore add the caveat to our d^8 formulation for **4** that a d^{10} configuration also has some merit.

To additionally probe this issue, a natural bond orbital (NBO) analysis[29] of **4** and **2** was performed. This analysis points to several features worth mentioning. The Wiberg bond index between two connected atoms provides a measure of their bond order. Given the $\{C-O-Na\}^+/\{C-O-SiMe_3\}^+$ analogy to which we drew attention above, it was of interest to compare this index for the C−O bond in the two species. In **4**, a Wiberg C−O bond index of 0.68 is calculated, compared with 1.62 for **2** (Table 2). These values can be compared with that of free CO, for which the Wiberg bond index has been calculated as 2.18. These values indicate that the π-bonding of CO has been obliterated in **4**, whereas substantial π-bond character remains in the C−O linkage of **2**. Accordingly, the Fe−C Wiberg bond index of **4** increases (1.86) in comparison to that of **2** (1.48) to compensate, implying stronger Fe−C π-bond character in **4**. As for the Mössbauer data, it is interesting to compare these indices with the analogous data calculated for the isostructural and isoelectronic species where N_2 is substituted for CO (Table 2).[5]

A Wiberg analysis of $(SiP^{iPr}_3)Fe(N_2Na(THF)_3)$ provides an N−N Wiberg index of 2.37, compared with 3.05 for free N_2. Hence, substantial π-bond character remains in $(SiP^{iPr}_3)Fe(N_2Na(THF)_3)$. Replacement of $Na(THF)_3^+$ by $SiMe_3^+$, as in $(SiP^{iPr}_3)Fe(N_2SiMe_3)$, attenuates the π-bonding (N−N Wiberg index =1.84), but not nearly to the same extent as occurs for the C−O linkage in **4**. Consistent with the X-ray data collected here and reported elsewhere,[5] the axial Fe−Si bond distance remains within a rather narrow range, regardless of the relative iron oxidation state and the axially bound ligand for both the N_2 and CO series. The largest discrepancy within the CO series concerns cation **5**, where the Fe−Si bond distance is 2.3245(7) Å, relative to the distance of 2.2586(8) Å in anion **2**. This difference may in part reflect less σ-donation from Fe to Si as the Fe center is oxidized. However, the triplet spin state in **5** relative to the singlet spin state in **2** may be the dominant factor. Consistent with the latter idea, the average of the Fe−P distances for triplet **5** (2.39 Å) is vastly greater than those for singlet **2** (2.19 Å). Indeed, the large difference in these Fe−P values underscores that the difference in Fe−Si bond distances is rather small between **2** and **5**. As should therefore be expected, the Fe−Si Wiberg bond indices for $Fe(N_2Na(THF)_3)$, $Fe(CONa(THF)_3)$, $Fe(N_2SiMe_3)$, and $Fe(COSiMe_3)$ supported by (SiP^{iPr}_3) also fall within a relatively narrow range, between 0.68 and 0.78, reflecting consistent bond character across the series.

The NBO analysis of **4** identifies an orbital that is σ-bonding between Fe and the Si atom of the (SiP^{iPr}_3) ligand. The bond orbital occupancy calculated distributes the Fe−Si σ-bond electron density between Fe and Si in ca. 60/40 ratio, respectively. For comparison, the electron pairs that are π-bonding between Fe and the $\{COSiMe_3\}^+$ ligand are also gleaned from the NBO analysis, where the π-electron density is ca. 70/30 weighted on

dx.doi.org/10.1021/ja109678y | J. Am. Chem. Soc. 2011, 133, 4438–4446

the Fe, and the σ-bond electron density is ca. 35/65 weighted on the C-atom. How one uses these data to aid the assignment of a d-electron configuration is not clear-cut. For example, two almost pure lone pairs reside on iron in **4** (Table 2), and, as noted above, two additional electron pairs are π-back-bonding to the $\{COSiMe_3\}^+$ but reside heavily on iron. Excluding the latter two electron pairs leads to a d^4 assignment, but such back-bonding electron pairs are typically accounted for in d-electron counts, and doing so here leads to a d^8 assignment that is better reflected in the Mössbauer data, which is most consistent with a low-valent iron center. But the a_1 symmetry orbital that is energetically within the d-orbital manifold and is σ-bonding between Fe and Si also resides largely on iron. Hence, it is somewhat arbitrary to exclude this final pair of electrons from the d-electron count. Including them instead provides a d^{10} configuration. Hence, the NBO analysis adds a degree of merit to the d^{10} configuration, where the mixed frontier orbital of a_1 symmetry resides largely on iron, as is also true of the two π-bonds between iron and carbon. A similar argument can be made for the diazenido species $(SiP^{iPr}_3)Fe(N_2SiMe_3)$. The placement of a filled a_1 orbital within the frontier set of orbitals, which arises from a strong orbital mixing scenario, therefore confuses a straightforward d-electron assignment for carbyne **4**. In this regard, the bonding situation finds analogy to that well appreciated in metal nitrosyl complexes and more recently metallaboratranes.[30,31] In the limit of the latter extreme, the iron center acts as a σ-donor to a cationic and Lewis acidic tetravalent silicon center.[32] In sum, the d^8 configuration for **4**, while not perfect, seems to fit best the collective data at hand and finds context by considering its electronic structure as similar to the large family of d^8 $Fe(CO)_xL_{5-x}$ structure types. This configuration also respects Pauling's principle of electroneutrality.[33]

Frenking and co-workers have studied extensively by theoretical means five-coordinate iron complexes that feature Fe−C multiple bonds.[34] Such species include, for example, $(CO)_4FeC$ with an axial bound C ligand and $I(CO)_3Fe(CH)$ with axially bound I and CH ligands. Both species are isoelectronic with **4**. NBO and Wiberg bond index analyses for these species point to bonding themes consistent with our own description of **4**. The key issue to highlight concerns the nature of the Fe−C bond. For both $(CO)_4FeC$ and $I(CO)_3Fe(CH)$, there is strong Fe−C multiple bonding, and as for the case of **4**, there is a σ-donor orbital best described as C→Fe and two π-bonds best described as Fe→C. Hence, even though ligands such as "C" and "CH" are commonly considered "Schrock-type" in high-valent metal complexes,[35,36] when matched with low-valent iron centers they are better formulated as "Fischer-type". It is this property, and hence reversal of polarization of the π-bonding in relation to a Schrock-type alkylidyne, that renders such ligands compatible with high d-count, low-valent metals. Were the axially bound C or CR ligand to be strongly π-donating, there would be a strong destabilization of filled d-orbitals.[37] While such destabilization leads to a favorable electronic structure for pseudotetrahedral $L_3Fe{\equiv}N_x$ species,[19] it perturbs favorable π-bonding in TBP structure types. For the Fe(C), Fe(CR), and $Fe(COSiMe_3)$ species under present discussion, however, there is net stabilization via π-back-bonding. Hence, when interacting with an L_4Fe or XL_3Fe fragment, both CH and $COSiMe_3$ are best formulated as "Fischer-type" ligands, and they give very similar Fe−C Wiberg indices (Wiberg index = 1.73 for $I(CO)_3Fe(CH)$ vs 1.86 for **4**). A similar overall formulation is true of the Fe−C interaction in $(CO)_4FeC$, though differences in the orbital makeup and net polarization of the Fe−C bonds arise due to rehybridization at carbon. Indeed, given Frenking's conclusions and the experimental data presented here for **4**, it is reasonable to hypothesize likely electronic stability for a hypothetical complex that is isoelectronic with **4**, namely "$\{(SiP^{iPr}_3)Fe(C)\}^-$", featuring a terminally bonded C-ligand.[38] Efforts are underway to explore the feasibility of such a species in our laboratories.

EXPERIMENTAL SECTION

General Considerations. All manipulations were carried out using standard Schlenk or glovebox techniques under a N_2 atmosphere. Unless otherwise noted, solvents were deoxygenated and dried by thoroughly sparging with Ar or N_2 gas followed by passage through an activated alumina column in the solvent purification system by SG Water, USA LLC. Non-halogenated solvents were tested with a standard purple solution of sodium benzophenone ketyl in tetrahydrofuran (THF) in order to confirm effective oxygen and moisture removal. $HSiP^{iPr}_3$,[4] $(SiP^{iPr}_3)Fe(CH_3)$,[5] $(SiP^{iPr}_3)Fe(N_2)$,[4,5] and $H(OEt_2)_2[B(3,5\text{-}C_6H_3(CF_3)_2)_4]$[39] were prepared according to literature procedures. All reagents were purchased from commercial vendors and used without further purification unless otherwise stated. Elemental analyses were performed by Midwest Microlab, LLC, Indianapolis, IN. Deuterated solvents were purchased from Cambridge Isotope Laboratories, Inc., degassed, and dried over activated 3-Å molecular sieves prior to use.

X-ray Crystallography Procedures. X-ray diffraction studies were carried out at the MIT Department of Chemistry X-ray Diffraction Facility on a Bruker Three-Circle Platform diffractometer, equipped with a CCD detector. Data were collected at 100 K using Mo Kα (λ = 0.71073 Å) or Cu Kα (λ = 1.54178 Å) radiation and solved using SHELX v. 6.14.[40] X-ray-quality crystals were grown as described in below. The crystals were mounted on a glass fiber or nylon loop with Paratone N oil. Structures were determined using direct methods with standard Fourier techniques using the Bruker AXS software package.

Spectroscopic Measurements. Varian Mercury-300, Varian Inova-500, and Bruker AVANCE-400 spectrometers were used to record ^1H, ^{13}C, ^{29}Si, and ^{31}P NMR spectra at ambient temperature unless otherwise indicated. ^1H and ^{13}C chemical shifts were referenced to the residual solvent peaks. ^{29}Si chemical shifts were referenced to external tetramethylsilane (TMS) (δ = 0 ppm). ^{31}P chemical shifts were referenced to external 85% phosphoric acid (δ = 0 ppm). Solution magnetic moments were determined by the method of Evans.[41] Optical spectroscopy measurements were taken on a Cary 50 UV/vis spectrophotometer using a 1-cm two-window quartz cell sealed with a standard closed cap purchased from Starna Cells, Inc. (catalog no. 1-Q-10-GL14-C). Infrared spectra were recorded on a BioRad FTS 3000 EXCALIBUR series FT-IR spectrometer using a solution IR cell or KBr pellet. X-band EPR spectroscopy measurements were taken on a Bruker EMS spectrometer. The low-temperature spectra were collected using a liquid nitrogen coldfinger dewar, and collected spectra were simulated using the W95EPR program.[42] ^{57}Fe Mössbauer spectra were measured with a constant acceleration spectrometer (SEE Co., Minneapolis, MN). Isomer shifts are quoted relative to Fe metal at room temperature. Data were analyzed and simulated with WMOSS software (Web Research Corp., Edina, MN).

Electrochemistry. Electrochemical measurements were carried out in a glovebox under a dinitrogen atmosphere in a one-compartment cell using a CH Instruments 600B electrochemical analyzer. A glassy carbon electrode was used as the working electrode, and platinum wire was used as the auxiliary electrode. The reference electrode was $Ag/AgNO_3$ in THF. The ferrocene couple Fc^+/Fc was used as an external reference. Solutions (THF) of electrolyte (0.3 M tetra-*n*-butylammonium hexafluorophosphate) and analyte were also prepared under an inert atmosphere.

dx.doi.org/10.1021/ja109678y |*J. Am. Chem. Soc.* 2011, 133, 4438–4446

DFT Calculations. Single-point calculations and NBO[43] analysis on **2** and **4** were run on the Gaussian03[44] suite of programs with the RB3LYP[45] level of theory with the 6-31++G** basis set for all atoms. Geometries for **2** and **4** were obtained from XRD data. To crudely assign the relative contribution of atomic orbitals to the HOMO, we calculated the Mulliken atomic spin density of a hypothetical $\{\mathbf{4}\}^+$ species. Mulliken atomic spin densities of the corresponding virtual cationic species of **2** and **4** were derived from the original single-point calculations of each singlet species by assigning **2** and **4** as doublet species without further optimization.

(SiP$^{i\mathrm{Pr}}_3$)Fe(CO) (1). (SiP$^{i\mathrm{Pr}}_3$)Fe(N_2) (0.055 g, 0.080 mmol) was dissolved in THF (20 mL) in a 50 mL sealable Schlenk tube. The reaction tube was taken out from the drybox and then connected to a Schlenk line and charged with CO gas (1 atm) after freeze−pump−thaw degassing three times. The reaction mixture was stirred overnight at room temperature (3 h at 60 °C). After all volatiles were removed by vacuum, the resulting product was dissolved in benzene (10 mL) and filtered through Celite. Product (SiP$^{i\mathrm{Pr}}_3$)Fe(CO) (**1**, 0.050 g, 0.072 mmol, 91%) was obtained as a yellow powder after removing volatiles by vacuum, washing with additional portions of pentane, and drying under vacuum. ^{1}H NMR (C_6D_6, ppm): 11.8, 7.2, 6.8, 4.6, 1.6, −3.8. Yellow X-ray-quality crystals were grown by evaporation of a benzene/pentane solution of **1**: TBP (τ = 0.97). UV−vis (THF, nm {cm^{-1} M^{-1}}): 260 {9400}, 313 {sh; ∼4700}, 375 {sh; 3100}, 990 {280}. μ_{eff} (C_6D_6, Evans method,[41] 20 °C): 2.0 μ_B. IR (ν_{CO}, cm^{-1}): 1848 (KBr pellet), 1852 (THF solution). Anal. Calcd for $C_{37}H_{54}FeOP_3Si$: C, 64.25; H, 7.87. Found: C, 64.18; H, 8.35.

(SiP$^{i\mathrm{Pr}}_3$)Fe(^{13}CO) (1-^{13}CO). (SiP$^{i\mathrm{Pr}}_3$)Fe(N_2) (0.100 g, 0.145 mmol) was dissolved in benzene (20 mL) in a 50 mL sealable Schlenk tube. The reaction tube was taken out from the drybox and then connected to a Schlenk line and charged with ^{13}CO gas (1 atm) after freeze−pump−thaw degassing three times. The reaction mixture was then stirred overnight at 60 °C. The resulting yellow solution was filtered through Celite, and all volatiles were removed by vacuum. Product (SiP$^{i\mathrm{Pr}}_3$)Fe(^{13}CO) (**1-^{13}CO**, 0.100 g, 0.144 mmol, 99%) was obtained as a yellow powder after washing with additional portions of pentane and drying under vacuum. Spectroscopic features in the ^{1}H NMR were identical to those for **1-^{13}CO**. IR ($\nu_{^{13}CO}$, cm^{-1}): 1806 (KBr pellet), 1808 (THF solution).

(SiP$^{i\mathrm{Pr}}_3$)Fe{CONa(THF)$_3$} (2). A dark green solution of sodium naphthalide was prepared by stirring a naphthalene solution (18 mg, 0.14 mmol) in THF (10 mL) over excess sodium metal (18 mg, 0.78 mmol) for 3 h at room temperature. The resulting sodium naphthalide solution was filtered away from any remaining sodium and added dropwise to the red solution of **1** (51 mg, 0.073 mmol) in THF (10 mL) at −35 °C, causing the color change to dark red over a period of several minutes. After stirring overnight at room temperature, the reaction mixture was filtered through Celite. Volatiles were removed under vacuum to give a dark red powder. The solid was collected on a medium-porosity glass frit and washed with pentane (5 mL × 2), benzene/pentane (1/5, 6 mL), and pentane (5 mL × 2). The resulting product, (SiP$^{i\mathrm{Pr}}_3$)Fe{CONa(THF)$_3$} (**2**, 67 mg, 0.072 mmol, 99%), was obtained as a dark red powder after drying under vacuum. ^{1}H NMR (THF-d_8, ppm): 8.3 (bs, 3H), 7.2 (d, J = 7.5 Hz, 3H), 6.9 (t, J = 6.9 Hz, 3H), 6.7 (bs, 3H), 3.6 (THF), 1.8 (THF), 1.0 (bs, 18H), 0.60 (bs, 18H). ^{31}P NMR (THF-d_8, ppm): 94.4 (s, at −70 °C). Dark red X-ray-quality crystals were grown by diffusion of pentane vapors into a THF solution of **2**: TBP (τ = 1.0). UV−vis (THF, nm {cm^{-1} M^{-1}}): 260 {13 000}, 330 {sh}, 424 {3700}, ∼990 {120}. IR (ν_{CO}, cm^{-1}): 1717 (KBr pellet), 1711 (THF solution).

(SiP$^{i\mathrm{Pr}}_3$)Fe{^{13}CONa(THF)$_3$} (2-^{13}CO). The same procedure used for **1-^{13}CO** was conducted. Spectroscopic features in the ^{1}H NMR were identical to those for **2**. ^{31}P NMR (THF-d_8, ppm; measured at −70 °C): 94.44. ^{13}C NMR (THF-d_8, ppm, measured at −70 °C): 239.6 (s). IR ($\nu_{^{13}CO}$, cm^{-1}): 1676 (KBr).

{Na(12-C-4)$_2$}{(SiP$^{i\mathrm{Pr}}_3$)Fe(CO)} (3). To a dark red solution of **2** (16 mg, 0.017 mmol) in THF (10 mL) was added a solution of 12-crown-4 (6 mg, 0.034 mmol) in THF (1 mL). The reaction mixture was stirred for 30 min at room temperature. The resulting darker solution was filtered through Celite. Volatiles were removed under vacuum to give a dark violet powder. The solid was collected on a medium porosity glass-frit and washed with pentane (3 mL×3). {Na(12-C-4)$_2$}{(SiP$^{i\mathrm{Pr}}_3$)Fe(CO)} (**3**, 18 mg, 0.017 mmol, 98%) was obtained as a dark crystalline solid from recrystallization with THF and pentane at room temperature. ^{1}H NMR (THF-d_8, ppm): 8.0 (bs, 3H), 7.1 (d, J = 6.9 Hz, 3H), 6.9 (m, 6H), 3.6 (32H, 12-C-4), 2.0 (bs, 6H), 0.9 (bs, 18H), 0.5 (bs, 18H). ^{31}P NMR (THF-d_8, ppm; measured at −70 °C): 94.4. Anal. Calcd for $C_{53}H_{86}FeNaO_9P_3Si$: C, 59.65; H, 8.12. Found: C, 59.72; H, 8.00. IR (ν_{CO}, cm^{-1}): 1757 (KBr pellet), 1779 (THF solution).

{Na(12-C-4)$_2$}{(SiP$^{i\mathrm{Pr}}_3$)Fe(^{13}CO)} (3-^{13}CO). The same procedure used for **2-^{13}CO** was conducted. Spectroscopic features in the ^{1}H NMR were identical to those for **3′**. ^{31}P NMR (THF-d_8, ppm; measured at −70 °C): 94.4. ^{13}C NMR (THF-d_8, ppm, measured at −70 °C): 239.7 (s). IR ($\nu_{^{13}CO}$, cm^{-1}): 1713 (KBr).

(SiP$^{i\mathrm{Pr}}_3$)Fe(COSiMe$_3$) (4). To a frozen solution of **2** (80 mg, 0.086 mmol) in THF (50 mL) was added trimethylsilyl triflate (20 mg, 0.090 mmol). The reaction mixture was slowly warmed to room temperature overnight. All volatiles were removed by vacuum, and the resulting red oil was dissolved in pentane. The red solution was filtered through Celite, and volatiles were removed by vacuum. The resulting product, (SiP$^{i\mathrm{Pr}}_3$)Fe(COSiMe$_3$) (**4**, 65 mg, 0.085 mmol, 99%),[46] was obtained as a red powder after drying under vacuum. ^{1}H NMR (C_6D_6, ppm): 8.14 (d, J = 7.2 Hz, 3H), 7.28 (d, J = 7.5 Hz, 3H), 7.22 (t, J = 6.9 Hz, 3H), 7.06 (t, J = 7.5 Hz, 3H), 2.40 (bs, 6H), 1.04 (m, 18H), 0.58 (bs, 18H), 0.34 (s, 9H). ^{31}P NMR (C_6D_6, ppm): 104.6 (s). ^{29}Si NMR (C_6D_6, ppm): 94.5 (q, $^2J_{SiP}$ = 40 Hz), 20.3 (s). Red X-ray-quality crystals were grown by evaporation of a pentane solution of **4** at −35 °C: TBP (τ = 0.98). UV−vis (THF, nm {cm^{-1} M^{-1}}): 260 {13 500}, 424 {4100}, 990 {70}. Anal. Calcd for $C_{40}H_{63}FeOP_3Si_2$: C, 62.81; H, 8.30. Found: C, 62.46; H, 7.70.

(SiP$^{i\mathrm{Pr}}_3$)Fe(^{13}COSiMe$_3$) (4-^{13}CO). The same procedure used for **2-^{13}CO** was conducted. Spectroscopic features in the ^{1}H NMR were identical to those for **4**. ^{31}P NMR (C_6D_6, ppm): 104.5 (d, $^2J_{CP}$ = 16.3 Hz). ^{13}C NMR (THF-d_8, ppm; measured at room temperature): 250.3 (q, $^2J_{CP}$ = 16.4 Hz). ^{29}Si NMR (C_6D_6, ppm; measured for 10 h at room temperature): 94.3 (dq, $^2J_{SiP}$ = 40 Hz, $^2J_{SiC}$ = 21 Hz), 20.0 (d, $^2J_{SiC}$ = 7 Hz).

(SiP$^{i\mathrm{Pr}}_3$)Fe(COSi^{i}Pr$_3$). To a frozen solution of **2** (38 mg, 0.041 mmol) in THF (20 mL) was added trimethylsilyl triflate (13 mg, 0.041 mmol). The reaction mixture was slowly warmed to room temperature overnight. All volatiles were removed by vacuum, and the resulting red oil was dissolved in pentane. The red solution was filtered through Celite, and volatiles were removed by vacuum. The resulting product, (SiP$^{i\mathrm{Pr}}_3$)Fe(COSi^{i}Pr$_3$) (35 mg, 0.040 mmol, 98%),[46] was obtained as a red powder after drying under vacuum. ^{1}H NMR (C_6D_6, ppm): 8.17 (d, J = 6.9 Hz, 3H), 7.34 (d, J = 7.2 Hz, 3H), 7.64 (t, J = 7.5 Hz, 3H), 7.09 (t, J = 7.5 Hz, 3H), 2.47 (bs, 6H), 1.48 (sep, J = 7.2 Hz, 3H), 1.22 (d, J = 7.2 Hz, 18H), 1.10 (m, 18H), 0.67 (bs, 18H). ^{31}P NMR (C_6D_6, ppm): 102.6 (s). ^{29}Si NMR (C_6D_6, ppm): 94.7 (q, $^2J_{SiP}$ = 42 Hz), 20.6 (s). UV−vis (THF, nm {cm^{-1} M^{-1}}): 260 {13 000}, 435 {4100}, 990 {68}.

{(SiP$^{i\mathrm{Pr}}_3$)Fe(CO)}{B(3,5-(CF$_3$)$_2$-C$_6$H$_3$)$_4$} (5). (SiP$^{i\mathrm{Pr}}_3$)Fe(CO) (**1**, 50 mg, 0.072 mmol) was dissolved in C_6H_6 (10 mL) and frozen at −35 °C. After H(OEt$_2$)$_2$[B(3,5-(CF$_3$)$_2$-C$_6$H$_3$)$_4$] (73 mg, 0.072 mmol) was added to the frozen solution, the mixture was vigorously stirred for 30 min at room temperature, resulting in precipitation of a blue solid. The precipitate was collected on a medium-porosity glass frit and washed with benzene (10 mL × 3) and pentane (10 mL × 3). The resulting powder, {(SiP$^{i\mathrm{Pr}}_3$)Fe(CO)}{B(3,5-(CF$_3$)$_2$-C$_6$H$_3$)$_4$} (**5**, 80 mg, 0.051 mmol, 72%), was dried under vacuum for a short time. ^{1}H NMR (THF-d_8, ppm): 15.2, 8.2, 7.6, 6.9, 4.6, −2.9, −6.2. Blue X-ray-quality crystals were grown by diffusion of pentane vapors into a THF/benzene

(1/1) solution of **5**: TBP (τ = 0.99). UV−vis (THF, nm {cm^{-1} M^{-1}}): 380 {sh, 980}, 470 {150}, 585 {140}, 700 {sh, 45}, 845 {20}, ∼1,100 {54}. μ_{eff} (THF-d_8, Evans method,[41] 20 °C): 2.7 μ_B. Anal. Calcd for $C_{69}H_{66}BF_{24}FeOP_3Si$: C, 53.30; H, 4.28. Found: C, 53.05; H, 4.20. IR (ν_{CO}, cm^{-1}): 1959 (KBr pellet), 1943 (THF solution). H_2(g) generated from the reaction was detected by GC analysis.

{(SiP$^{iPr}_3$)Fe(^{13}CO)}{B(3,5-(CF$_3$)$_2$-C$_6$H$_3$)$_4$} (5-^{13}CO). The same procedure used for **1**-^{13}**CO** was conducted. Spectroscopic features in the ^{1}H NMR were identical to those for **5**. IR ($\nu_{^{13}CO}$, cm^{-1}): 1915 (KBr).

{(SiP$^{iPr}_3$)Fe(Cl)}{B(3,5-(CF$_3$)$_2$-C$_6$H$_3$)$_4$}. (SiP$^{iPr}_3$)Fe(CH$_3$) (21 mg, 0.031 mmol) was dissolved in CH_2Cl_2 (5 mL) and cooled to −35 °C. After H(OEt$_2$)$_2$[B(3,5-(CF$_3$)$_2$-C$_6$H$_3$)$_4$] (30 mg, 0.030 mmol) was added to the red solution, the mixture was vigorously stirred for 30 min at room temperature, resulting in a dark green solution. After volatiles were removed by vacuum, the resulting powder was collected on a medium-porosity glass frit and washed with benzene (10 mL × 3) and pentane (10 mL × 3). The resulting product, {(SiP$^{iPr}_3$)Fe(Cl)}{B(3,5-(CF$_3$)$_2$-C$_6$H$_3$)$_4$} (30 mg, 0.019 mmol, 65%), was then dried under vacuum. ^{1}H NMR (CD_2Cl_2, ppm): 11.26, 8.27, 7.69, 7.54, 6.85, −13.04. Dark red X-ray-quality crystals were grown by diffusion of pentane vapors into a CH_2Cl_2 solution of {(SiP$^{iPr}_3$)Fe(Cl)}{B(3,5-(CF$_3$)$_2$-C$_6$H$_3$)$_4$}: TBP (τ = 1.0). UV−vis (THF, nm {cm^{-1} M^{-1}}): 387 {4500}, 430 {sh, 3300}, 512 {930}, 596 {670}, 841 {470}. μ_{eff} (CD_2Cl_2, Evans method,[41] 20 °C): 3.9 μ_B. Anal. Calcd for $C_{68}H_{66}BClF_{24}FeP_3Si$: C, 52.28; H, 4.26. Found: C, 52.31; H, 4.39.

■ ASSOCIATED CONTENT

Supporting Information. Characterization data for **1**−**5**; crystallographic data for **1**, **2**, **4**, and **5** (CIF); details of DFT calculations; complete ref 44. This material is available free of charge via the Internet at http://pubs.acs.org.

■ AUTHOR INFORMATION

Corresponding Author
jpeters@caltech.edu

■ ACKNOWLEDGMENT

We acknowledge the NSF (CHE-0750234) for financial support. Dr. Neal P. Mankad provided assistance with XRD analyses, and Prof. Theodore A. Betley provided access to a Mössbauer spectrometer at Harvard University. Prof. Michael T. Green and Dr. Marc-Etienne Moret are acknowledged for insightful discussions concerning theoretical data. We also want to express gratitude to a reviewer for suggestions that improved the reported X-ray data.

■ REFERENCES

(1) (a) Mindiola, D. J.; Hillhouse, G. L. *J. Am. Chem. Soc.* **2001**, *123*, 4623–4624. (b) Jenkins, D. M.; Betley, T. A.; Peters, J. C. *J. Am. Chem. Soc.* **2002**, *124*, 11238–11239. (c) Brown, S. D.; Betley, T. A.; Peters, J. C. *J. Am. Chem. Soc.* **2003**, *125*, 322–323. (d) Dai, X. L.; Warren, T. H. *J. Am. Chem. Soc.* **2004**, *126*, 10085–10094. (e) Ni, C. B.; Fettinger, J. C.; Long, G. J.; Brynda, M.; Power, P. P. *Chem. Commun.* **2008**, 6045–6047. (f) Shay, D. T.; Yap, G. P. A.; Zakharov, L. N.; Rheingold, A. L.; Theopold, K. H. *Angew. Chem., Int. Ed.* **2005**, *44*, 1508–1510. (g) Ingleson, M. J.; Pink, M.; Fan, H.; Caulton, K. G. *J. Am. Chem. Soc.* **2008**, *130*, 4262–4267.

(2) (a) Kieber-Emmons, M. T.; Riordan, C. G. *Acc. Chem. Res.* **2007**, *40*, 618–625. (b) Kitiachvili, K. D.; Mindiola, D. J.; Hillhouse, G. H. *J. Am. Chem. Soc.* **2004**, *126*, 10554–10555.

(3) (a) Lu, C. C.; Saouma, C. T.; Day, M. W.; Peters, J. C. *J. Am. Chem. Soc.* **2007**, *129*, 4–5. (b) Laitar, D. S.; Müller, P.; Sadighi, J. P. *J. Am. Chem. Soc.* **2005**, *127*, 17196–17197. (c) Sadique, A. R.; Brennessel, W. W.; Holland, P. L. *Inorg. Chem.* **2008**, *47*, 784–786. (d) Benson, E. E.; Kubiak, C. P.; Sathrum, A. J.; Smieja, J. M. *Chem. Soc. Rev.* **2009**, *38*, 89–99.

(4) (a) Mankad, N. P.; Whited, M. T.; Peters, J. C. *Angew. Chem., Int. Ed.* **2007**, *46*, 5768–5771. (b) Whited, M. T.; Mankad, N. P.; Lee, Y.; Oblad, P. F.; Peters, J. C. *Inorg. Chem.* **2009**, *48*, 2507–2517.

(5) Lee, Y; Mankad, N. P.; Peters, J. C. *Nature Chem.* **2010**, *2*, 558–565.

(6) Cummins, C. C. *Chem. Commun.* **1998**, 1777–1786.

(7) Lee, C. L.; Hu, Y.; Ribbe, M. W. *Science* **2010**, 642.

(8) Fischer, E. O.; Kreis, G.; Kreiter, C. G.; Müller, J.; Huttner, G.; Lorenz, H. *Angew. Chem., Int. Ed. Engl.* **1973**, *12*, 564.

(9) *Transition Metal Carbyne Complexes*; Kreissel, F. R., Ed.; Kluwer Academic Publishers: Dordrecht, The Netherlands, 1993.

(10) (a) Fischer, E. O.; Schneider, J.; Neugebauer, D. *Angew. Chem., Int. Ed. Engl.* **1984**, *23*, 820–821. A related iron complex that was spectroscopically but not structurally characterized has also been described:(b) Anderson, S.; Hill, A. F. *J. Organomet. Chem.* **1990**, *394*, C24–C26. (c) Anderson, S.; Hill, A. F.; Ng, Y. T. *Organometallics* **2000**, *19*, 15–21.

(11) (a) Joslin, F. L.; Stobart, S. R. *J. Chem. Soc., Chem. Commun.* **1989**, 504–505. (b) Hendriksen, D. E.; Oswald, A. A.; Ansell, G. B.; Leta, S.; Kastrup, R. V. *Organometallics* **1989**, *8*, 1153–1157.

(12) For examples of Fe(I)−CO species, see:(a) Kisko, J. L.; Hascall, T.; Parkin, G. *J. Am. Chem. Soc.* **1998**, *120*, 10561–10562. (b) MacBeth, D. E.; Harkins, S. B.; Peters, J. C. *Can. J. Chem.* **2005**, *83*, 332–340. (c) Mock, M. T.; Popescu, C. V.; Yap, G. P. A.; Dougherty, W. G.; Riordan, C. G. *Inorg. Chem.* **2008**, *47*, 1889–1891.

(13) Addison, A. W.; Rao, T. N.; Reedijk, J.; Vanrijn, J.; Verschoor, G. C. *J. Chem. Soc., Dalton Trans.* **1984**, 1349–1356.

(14) (a) Ayoko, G. A.; Eaborn, C.; Hitchcock, P. B. *Organometallics* **1995**, *14*, 4960–4961. (b) Al-Juaid, S. S.; Al-Nasr, A. A.; Ayoko, G. A.; Eaborn, C.; Hitchcock, P. *J. Organomet. Chem.* **1995**, *488*, 155–160.

(15) (a) Vrtis, R. N.; Rao, C. P.; Warner, S.; Lippard, S. J. *J. Am. Chem. Soc.* **1988**, *110*, 2669–2670. (b) Vrtis, R. N.; Liu, S.; Rao, S. P.; Bott, S. G.; Lippard, S. J. *Organometallics* **1991**, *10*, 275–285. (c) Protasiewicz, J. D.; Masschelein, A.; Lippard, S. J. *J. Am. Chem. Soc.* **1993**, *115*, 808–810. (d) Sakaba, H.; Yoshida, M.; Kabuto, C.; Kabuto, K. *J. Am. Chem. Soc.* **2005**, *127*, 7276–7277.

(16) (a) Stang, P. J.; Crittell, C. M.; Arif, A. M.; Karni, M.; Apeloig, Y. *J. Am. Chem. Soc.* **1991**, *113*, 7461–7470. (b) Gleiter, R.; Werz, D. B.; Rominger, F.; Zhutov, E.; Zefirov, N. S.; Proskurnina, M. V. *Eur. J. Org. Chem.* **2007**, 5834–5839.

(17) A Wiberg bond index analysis suggests strong multiple bond character in the Fe−C linkage (bond index = 1.85) and single bond character at the C−O linkage (bond index = 0.68) of **4**. See Supporting Information for details.

(18) Parkin, G. In *Comprehensive Organometallic Chemistry*; Crabtree, R. H., Mingos, D. M. P., Eds.; Elsevier: Amsterdam, 2007; Vol. 1, pp 1−57.

(19) (a) Betley, T. A.; Peters, J. C. *J. Am. Chem. Soc.* **2003**, *125*, 10782–10783. (b) Betley, T. A.; Peters, J. C. *J. Am. Chem. Soc.* **2004**, *126*, 6252–6254. (c) Hendrich, M. P.; Gunderson, W.; Behan, R. K.; Green, M. T.; Mehn, M. P.; Betley, T. A.; Lu, C. C.; Peters, J. C. *Proc. Natl. Acad. Sci. U.S.A.* **2006**, *103*, 17107–17112. (d) Thomas, C. M.; Mankad, N. P.; Peters, J. C. *J. Am. Chem. Soc.* **2006**, *128*, 4956–4957. (e) Vogel, C.; Heinemann, F. W.; Sutter, J.; Anthon, C.; Meyer, K. *Angew. Chem., Int. Ed.* **2008**, *47*, 2681–2684. (f) Scepaniak, J. J.; Young, J. A.; Bontchev, R. P.; Smith, J. M. *Angew. Chem., Int. Ed.* **2009**, *48*, 3158–3160.

(20) Detrich, J. L.; Konecny, R.; Vetter, W. M.; Doren, D.; Rheingold, A. L.; Theopold, K. H. *J. Am. Chem. Soc.* **1996**, *118*, 1703–1712.

(21) (a) Gibb, T. C. *Principles of Mössbauer Spectroscopy*; Wiley: New York, 1976. (b) Bancroft, G. M. *Mössbauer Spectroscopy—An Introduction for Inorganic and Geochemists*; McGraw-Hill: London, 1971.

(22) (a) Clark, M. G.; Cullen, W. R.; Garrod, R. E. B.; Maddock, A. G.; Sams, J. R. *Inorg. Chem.* **1973**, *12*, 1045. (b) Pribula, C. G.; Brown, T. L.; Munck, E. *J. Am. Chem. Soc.* **1974**, *96*, 4149.

(23) Sosinsky, B. A.; Norem, N.; Shong, R. G. *Inorg. Chem.* **1982**, *21*, 4229–4233.
(24) Collins, R. L.; Pettit, R. *J. Chem. Phys.* **1963**, *39*, 3433.
(25) Sosinsky, B. A.; Norem, N.; Shong, R. G. *Inorg. Chem.* **1982**, *21*, 4229–4233.
(26) Dias, G. H. M.; Morigaki, M. K. *Polyhedron* **1992**, *11*, 1629–1636.
(27) Schmidt, G.; Balk, H. J. *J. Organomet. Chem.* **1974**, *80*, 257.
(28) To crudely estimate the relative contribution of atomic orbitals to the HOMO, we calculated the Mulliken atomic spin density of the hypothetical $\{\mathbf{4}\}^{+}$.
(29) (a) Feed, A. E.; Curtiss, L. A.; Weinhold, F. *Chem. Rev.* **1988**, 899.(b) Weinhold, F.; Landis, C. R. *Valency and Bonding: A Natural Bond Ordital Donor−Acceptor Perspective*; Cambridge University Press: New York, 2005.
(30) (a) Enemark, J. H.; Feltham, R. D. *Coord. Chem. Rev.* **1974**, *13*, 339–406.(b) Richter-Addo, G. B.; Legzdin, P. *Metal Nitrosyls*; Oxford University Press: Oxford, UK, 1992.
(31) (a) Hill, A. F. *Organometallics* **2006**, *25*, 4741–4743. (b) Parkin, G. *Organometallics* **2006**, *25*, 4744–4747. (c) Figueroa, J. S.; Melnick, J. G.; Parkin, G. *Inorg. Chem.* **2006**, *45*, 7056–7058. (d) Sircoglou, M.; Bontemps, S.; Bouhadir, G.; Saffon, N.; Miqueu, K.; Gu, W.; Mercy, M.; Chen, C.-H.; Foxman, B. M.; Maron, L.; Ozerov, O. V.; Bourissou, D. *J. Am. Chem. Soc.* **2008**, *130*, 16729–16738. (e) Kuzu, I.; Krummenacher, I.; Meyer, J.; Armbruster, F.; Breher, F. *Dalton Trans.* **2008**, 5836–5865. (f) Braunschweig, H.; Dewhurst, R. D.; Schneider, A. *Chem. Rev.* **2010**, *110*, 3924–3957.
(32) (a) Gualco, P.; Lin, T.-P.; Sircoglou, M.; Mercy, M.; Ladeira, S.; Bouhadir, G.; Pèrez, L. M.; Amgoune, A.; Maron, L.; Gabbaï, F.; Bourissou, D. *Angew. Chem., Int. Ed.* **2009**, *48*, 9892–9895. (b) Corey, J. Y.; Braddock-Wilking, J. *Chem. Rev.* **1999**, *99*, 175–292.
(33) Pauling, L. *J. Phys. Chem.* **1952**, *56*, 361–365.
(34) (a) Chen, Y.; Petz, W.; Frenking, G. *Organometallics* **2000**, *19*, 2698–2706. (b) Krapp, A.; Pandey, K. K.; Frenking, G. *J. Am. Chem. Soc.* **2007**, *129*, 7596–7610.
(35) Schrock, R. R. *J. Am. Chem. Soc.* **1974**, *96*, 6796–6797.
(36) McLain, S. J.; Wood, C. D.; Messerle, L. W.; Schrock, R. R.; Hollander, F. J.; Youngs, W. J.; Churchill, M. R. *J. Am. Chem. Soc.* **1978**, *100*, 5962–5964.
(37) Mankad, N. P.; Müller, P.; Peters, J. C. *J. Am. Chem. Soc.* **2010**, *132*, 4083–4085.
(38) (a) Peters, J. C.; Odom, A. L.; Cummins, C. C. *J. Chem. Soc., Chem. Commun.* **1997**, 1995. (b) Carlson, R. G.; Gile, M. A.; Heppert, J. A.; Mason, M. H.; Powell, D. R.; Velde, D. V.; Vilain, J. M. *J. Am. Chem. Soc.* **2002**, *124*, 1580–1581.
(39) (a) Yakelis, N. A.; Bergman, R. G. *Organometallics* **2005**, *24*, 3579–3581. (b) Brookhart, M.; Grant, B.; Volpe, A. F., Jr. *Organometallics* **1992**, *11*, 3920–3922.
(40) Sheldrick, G. M. *Acta Crystallogr. A* **2008**, *64*, 112–122.
(41) (a) Evans, D. F. *J. Chem. Soc.* **1959**, 2003–2005. (b) Sur, S. K. *J. Magn. Reson.* **1989**, *82*, 169–173.
(42) Neese, F. *QCPE Bull.* **1995**, *15*, 5.
(43) (a) Feed, A. E.; Curtiss, L. A.; Weinhold, F. *Chem. Rev.* **1988**, 899.(b) Weinhold, F.; Landis, C. R. *Valency and Bonding: A Natural Bond Orbital Donor-Acceptor Perspective*; Cambridge University Press: New York, 2005.
(44) Frisch, M. J.; et al. *Gaussian 03*, Revision C.02; Gaussian, Inc.: Wallingford, CT, 2004.
(45) (a) Becke, A. D. *J. Chem. Phys.* **1993**, *98*, 5648. (b) Lee, C.; Yang, W.; Parr, R. G. *Phys. Rev. B* **1988**, *37*, 785.
(46) A trace amount of **1** can be seen in the ^{1}H NMR spectrum.